ELSEVIER

International Journal of Mass Spectrometry 226 (2003) 85–106

International Journal of Mass Spectrometry

www.elsevier.com/locate/ijms

Molecular dynamics simulations of matrix-assisted laser desorption—connections to experiment

Leonid V. Zhigilei[a,1], Yaroslava G. Yingling[b], Tatiana E. Itina[c], Tracy A. Schoolcraft[d], Barbara J. Garrison[b,*]

[a] *Department of Materials Science and Engineering, 116 Engineer's Way, University of Virginia, Charlottesville, VA 22904, USA*
[b] *Department of Chemistry, 152 Davey Laboratory, Penn State University, University Park, PA 16802, USA*
[c] *Université d'Aix Marseille II, Campus de Luminy, Case 917, 13288, Marseille, France*
[d] *Department of Chemistry, Shippensburg University, 1871 Old Main Drive, Shippensburg, PA 17257, USA*

Received 30 July 2001; accepted 30 June 2002

In honor of Franz Hillenkamp's 65th birthday.

Abstract

The molecular dynamics (MD) simulation technique has been applied to investigate fundamental aspects of matrix-assisted laser desorption. In this paper, we focus on direct comparisons of the results from the simulations with experimental data and on establishing links between the measured or calculated parameters and the basic mechanisms of molecular ejection. The results on the fluence dependence of the ablation/desorption yields and composition of the ejected plume are compared with mass spectrometry and trapping plate experiments. Implications of the prediction of a fluence threshold for ablation are discussed. The strongly forward-peaked velocity and angular distributions of matrix and analyte molecules, predicted in the simulations, are related to the experimental distributions. The shapes and amplitudes of the acoustic waves transmitted from the absorption region through the irradiated sample are compared to recent photoacoustic measurements and related to the ejection mechanisms. The conformational changes during plume evolution and the ejection velocities of analyte molecules are studied and the directions for future investigations are discussed. Finally, we demonstrate that the MD simulation technique can be used to model other processes relevant to mass spectrometry applications, such as laser disintegration of aerosol particles and laser ablation in the presence of photochemical reactions.

Keywords: Ablation; MALDI; Molecular dynamics

1. Introduction

Matrix-assisted laser desorption ionization (MALDI) mass spectrometry [1,2] is a leading technique for performing mass analysis of nonvolatile organic and biological molecules as evidenced by other articles in this special issue in honor of Franz Hillenkamp. Although there are a plethora of applications, the theoretical and computational approaches for understanding the associated physical phenomena have only in the past few years begun to catch up with experimental understanding. Initially, analytical theories and models provided insights into the mechanisms of MALDI

* Corresponding author.
[1] Co-corresponding author.
E-mail addresses: bjg@chem.psu.edu (B.J. Garrison), lz2n@virginia.edu (L.V. Zhigilei).

1387-3806/02/$ – see front matter
PII S1387-3806(02)00962-4

[3–7]. The complexity and diversity of the processes involved in laser ablation of a molecular matrix, namely, laser excitation of absorbing molecules, energy transfer from the excited molecules into the internal and translational modes of the surrounding molecules, material disintegration, and prompt forward ejection along with interactions in the plume, however, hinder a comprehensive analytical description of all the important processes. Previously, even a qualitative picture of laser ablation could not be established. Analytical models based on such diverse assumptions as the thermo-fluctuational sublimation of molecules from the surface (surface vaporization) [6,8], explosive bulk desorption due to a nonequilibrium phase transition [4,9] or critical pressure gradient [3,10] were used to explain the experimental observations.

Subsequently, there were a few attempts to address the laser desorption/ablation phenomena by conventional atomic level molecular dynamics (MD) method [11–15]. These works have clearly demonstrated the attractive sides of the MD method. Severe limitations on size of the computational cell and time of the simulation, however, make it difficult to relate simulation results to real experimental conditions. In addition, the analysis of the ejected plume in terms of velocity, angular, and cluster distributions requires a considerably bigger system and a longer simulation time so that statistically significant data can be obtained.

In order to conduct a comprehensive study of the laser ablation phenomena associated with MALDI at an expanded time and length scales, we developed a mesoscopic model. Our initial goals for the model were as follows:

- Identify the processes that distinguish desorption from ablation and explain a fluence threshold that separates the two regimes of molecular ejection.
- Investigate the dependence of the processes leading to the molecular ejection on irradiation conditions such as laser fluence and pulse width, and optical penetration depth.
- Predict the ablation plume composition for different irradiation conditions.
- Reveal the physics leading to the forward-peaked velocity distributions of matrix and analyte molecules and investigate the mass dependence of the ejection velocities.
- Finally, the model has to be sufficiently flexible so that inhomogeneous materials and various laser excitation modes such as thermal and photochemical events can be investigated.

The MD approach is an ideal candidate for meeting these stated goals. The advantage of the MD method is that only details of the microscopic interactions need to be specified and no assumptions are made about the character of the processes under study. Moreover, the MD method is capable of providing a complete microscopic description of the dynamical processes involved in laser ablation. As stated earlier, however, the challenges in using an MD description of laser ablation are the limitations of time and length scales.

We have developed a breathing sphere model aimed at overcoming these limitations [16–28]. The novel feature of the breathing sphere model is an approximate representation of the internal atomic motions, thus we can significantly expand the time and length scales of the simulation yet still reproduce a realistic rate of the vibrational relaxation of excited molecules. Details of the breathing sphere model are given in a number of publications [16,19,22,25]. The focus of this article is on direct comparisons of the results from the simulations with experimental data. The breathing sphere model in its current implementation is applicable only to the desorption/ablation phenomena and does not include ionization processes.

The basic mechanisms of molecular ejection for a pure matrix system are discussed first and the results on the fluence dependence of the desorption/ablation yields and composition of the ejected plume are compared with trapping plate and mass spectrometry experiments. We then analyze our initial simulations that incorporate analyte molecules and discuss the ramifications of the predictions for MALDI. The initial velocity and angular distributions of matrix molecules are calculated and related to experimentally measured distributions. The predictions of the

breathing sphere model on the shapes and amplitudes of the acoustic waves transmitted from the absorption region through the MALDI sample are presented and compared with recent photoacoustic measurements. Finally, we demonstrate that the MD approach can be used to model other processes relevant to MS applications, such as laser disintegration of aerosol particles and laser ablation in the presence of photochemical reactions.

2. Computational model

In this section we review the basic features of the breathing sphere model developed for MD simulations of laser ablation of organic solids. Then we describe the computational setup and explain the choices of the irradiation parameters used in the simulations.

2.1. Breathing sphere model

In this section we give only a brief review of the breathing sphere model that is described in more detail elsewhere [16,19]. The model assumes that each molecule (or appropriate group of atoms) can be represented by a single particle. The parameters of interparticle interaction are chosen to reproduce the properties of the material, in this case, a molecular solid. In order to simulate molecular excitation by photon absorption and vibrational relaxation of the excited molecules, an additional internal degree of freedom is attributed to each molecule. This internal degree of freedom, or breathing mode, is realized by allowing each particle to change its size during the simulation. The parameters of a potential function ascribed to the internal motion can be used to change the characteristic frequency of the breathing mode and to affect the coupling between internal and translational molecular motions. In effect, one can control the rate of the conversion of internal energy of the molecules excited by the laser to the translational and internal motion of the other molecules. The rate of the vibrational relaxation of excited molecules is an input parameter in the model and can be either estimated from experimental data [29,30] or modeled with atomistic [14,31,32] or ab initio [33] MD simulations.

The laser irradiation is simulated by vibrational excitation of molecules that are randomly chosen during the laser pulse duration within the penetration depth appropriate for a given wavelength. Vibrational excitation is modeled by depositing a quantum of energy equal to the photon energy into the kinetic energy of internal motion of a given molecule. An alternative result of the photon absorption is photofragmentation of the excited molecule into fragments that can subsequently react. An increase of the volume occupied by the reaction products can be simulated by either an increase of the equilibrium radii of spherical particles representing the excited molecules [16,19,34,35] or by introducing several smaller particles representing the reaction products [36,37].

The total number of photons entering the simulations during the laser pulse is determined by the laser fluence, i.e., the incident laser energy per unit surface area. The absorption probability can be modulated by Lambert–Beer's law to reproduce the exponential attenuation of the laser light with depth or can be restricted to a certain component within a complex material.

Since in this model each molecule is represented by a single particle, the system size can be sufficiently large to reproduce the collective dynamics leading to laser ablation and damage. Moreover, since explicit atomic vibrations are not followed, the time-step in the numerical integration of the equations of motion can be much longer and the dynamics in the irradiated sample can be followed for as long as nanoseconds. One effect, however, that is difficult to simulate directly even within the coarse-grained breathing sphere MD model is propagation of the laser-induced photoacoustic wave in the direction away from the surface. Simply put, we would have to use too many molecules in the simulation to follow the long-term propagation of the pressure wave in the sample.

In order to avoid artifacts due to the pressure wave reflection at the bottom of the sample, we have developed a simple and computationally efficient boundary condition based on analytical evaluation of the forces

acting at the molecules in the boundary region from the outer "infinite medium" [23]. In this approach terminating forces are applied to the molecules in the boundary region. In the calculation of the terminating forces, which are updated at each integration step, we take into account three effects, namely, the static forces that mimic interaction with molecules beyond the computational cell, the forces due to the direct laser energy absorption in and around the boundary region during the laser pulse, and the forces due to the pressure wave propagation through the boundary region. The contribution of the pressure wave to the terminating force is calculated based on the traveling wave equation and is proportional to the instantaneous velocity of the boundary [23].

2.2. Simulation setup

The system chosen for modeling of laser ablation is a molecular solid or matrix used in mass spectrometry MALDI experiments. The parameters of the intermolecular potential are chosen to represent the van der Waals interaction in a molecular solid with the cohesive energy of 0.6 eV, elastic bulk modulus of ∼5 GPa, and density of 1.2 g/cm^3. A mass of 100 Da is attributed to each molecule. An amorphous molecular solid prepared by melting of a close packed crystal and subsequent quenching from the melt [38] is used in the simulation [16,19]. Typically we use computational cells of dimensions 10 nm × 10 nm × 100 nm (70,526 molecules) or 10 nm × 10 nm × 180 nm (126,950 molecules). Test simulations with larger computational cells are performed in order to make certain that the simulation results are not affected by the finite size of the computational cell. Periodic boundary conditions in the directions parallel to the surface are imposed. These conditions simulate the situation in which the laser spot diameter is large compared to the penetration depth so that the effects of the edges of the laser beam are neglected. At the bottom of the MD computational cell, we apply the dynamic boundary condition mentioned earlier.

Even though the breathing sphere model allows us to model larger systems for longer times than atomistic simulations, these calculations are still computationally intensive. A simulation for 1 ns of time for one average fluence with the 126,950 molecule system takes ∼2 weeks on an IBM four-way SMP node. The calculations mentioned at the end of this article that include photochemical events takes approximately 50% more computer time.

2.3. Irradiation regimes

The laser irradiation at a wavelength of 337 or 248 nm is simulated and an exponential decrease of the absorption probability with depth in accordance with Beer's law is applied. In the simulations with vibrational relaxation of the excited molecules all the laser energy is available for translational and internal motions of the breathing spheres, thus only the total fluence and not the wavelength is important. An absorption depth used in the simulations, typically 50 nm, is in the range of the values appropriate for strongly absorbing matrixes used in ultra violet (UV)-MALDI [39]. The values of the laser pulse duration, τ_p, of 15 and 150 ps are chosen in order to make sure that simulations are performed in two distinct irradiation regimes, stress confinement and thermal confinement [25].

For the system used in the simulations, the pulse duration of 150 ps is short relative to the characteristic thermal diffusion time across the absorption depth, τ_{th} ∼10 ns, but longer than the time of mechanical equilibration of the absorbing volume, τ_s ∼20 ps [25]. Thus, the simulations with 150 ps pulses are performed in the regime of thermal confinement but not thermoelastic stress confinement. This regime is also characteristic for UV-MALDI. In particular, an estimated thermal relaxation time of 10 ns is given in Ref. [8] for typical UV-MALDI conditions, which is longer than a typical pulse width of several nanoseconds. It has been demonstrated recently by Dreisewerd et al. [40] that in the regime of thermal confinement the amount of energy deposited by the laser pulse rather than the pulse duration determines the desorption/ablation process. A similar conclusion was reached due to experiments by Riahi et al. [41]. Therefore, even though

the pulse duration of 150 ps is an order of magnitude shorter than the pulses commonly used in MALDI, a qualitative comparison between the simulation results and UV-MALDI experimental data is justified.

For the 15 ps laser pulse the condition for stress confinement, $\tau_p \leq \tau_s$, is satisfied. In this case a high thermoelastic pressure can be expected to result from the fast energy deposition in the absorption region leading to an increasing role of photomechanical effects in material ejection. The results from this set of simulations can help in understanding of the microscopic mechanisms responsible for energetically efficient ablation in a number of applications, such as infra red (IR)-MALDI and laser surgery, where the regime of at least partial stress confinement is realized [42–47].

3. Results and comparisons to experiment

The discussion of the simulation results given in this section starts from the mechanisms of material ejection and their dependence on the irradiation parameters. The information on the ejection mechanisms is then related to the parameters of the desorption/ablation that can be measured experimentally. Cluster composition of the plume, parameters of the ejected analyte molecules, velocity and angular distribution of matrix molecules in the plume, shapes and amplitudes of the laser-induced acoustic waves are analyzed and related to the available experimental data. The direct comparison of the results from the simulations with experimental data allows us to verify the model and to establish links among the variety of parameters of the ejection process and the mechanisms of molecular ejection. At the end of this section, we briefly discuss several example problems that illustrate the diversity of systems and processes that can be addressed by MD simulation technique.

3.1. Mechanisms

The dependences of the total yield on laser fluence for the 150 and 15 ps laser pulses are similar as shown in Fig. 1. For both thermal and stress confinement, there are two distinct regimes of molecular ejection separated by a well-defined threshold fluence, F_{th} [16,17,19,22,25]. At the threshold fluence, the ejection mechanism changes from desorption at low fluences to ablation at higher fluences and the total yield increases abruptly. Large molecular clusters become a major constituent of the plume above the ablation threshold. The inserted snapshots from the simulation are placed at approximately the corresponding fluences.

3.1.1. Desorption

Below the ablation threshold primarily individual molecules are emitted from the surface, as shown in the picture in the lower left corner of Fig. 1. At the lowest fluences where we detect ejected molecules, the surface temperature reaches 735 K, slightly below the melting temperature of the model material, ~750 K. Therefore, the molecular ejection can be attributed to the desorption from a solid. As the fluence increases towards the ablation threshold, the near-surface region melts and desorption occurs from a liquid surface region [10,21]. We find that the dependence of the desorption yield on laser fluence F can be well described by an Arrhenius-type expression [3,8,22,25],

$$N = A \exp\left[-\frac{E_s^*}{k_B\,(T_0 + BF)}\right], \quad \text{for} \quad F < F_{th} \qquad (1)$$

where N is the number of molecules desorbed during the time of a simulation, E_s^* is an activation energy, A is a pre-exponential or frequency factor, B is a factor that describes the conversion of the deposited energy into an increase of temperature of the surface [22], T_0 is the initial temperature [48], and k_B is Boltzmann's constant. Eq. (1) provides a good fit of the desorption yield with the same activation energy E_s^* of 0.46 eV for both 150 and 15 ps laser pulses. The dashed line in Fig. 1 is from Eq. (1). The thermal desorption model thus provides an adequate description of the molecular ejection at low laser fluences and the process is not sensitive to pulse duration.

3.1.2. Ablation

The total amount of the ejected material increases at the threshold fluences by more than an order of

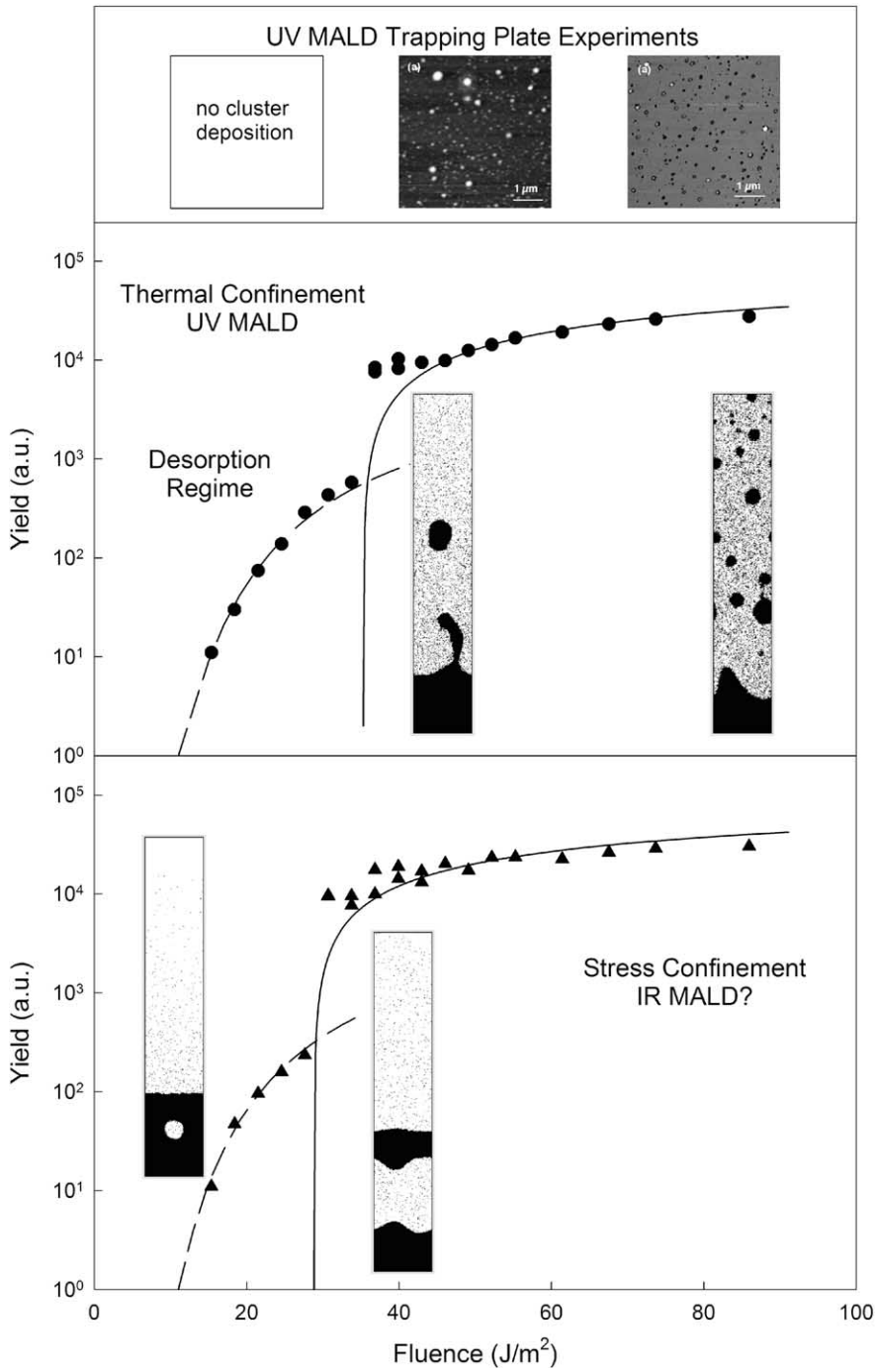
UV MALD Trapping Plate Experiments
no cluster deposition
(a)
(d)
1 μm
1 μm
Thermal Confinement
UV MALD
Desorption
Regime
Yield (a.u.)
Stress Confinement
IR MALD?
Fluence (J/m2)

magnitude, as can be seen in Fig. 1. This stepwise transition from ejection of about a monolayer of molecules in the desorption regime to a collective ejection, or ablation, of a significant part of the absorbing volume is a reflection of qualitative changes in the ejection mechanism. The thermal desorption model is not valid in the ablation regime and a different analytical description of the yield vs. fluence dependence should be used. We find that, for both pulse durations used in the present work, the amount of material ejected in the ablation regime can be relatively well described by a simple model in which the ablation depth follows the laser energy deposition and all material that absorbs an energy density higher than a critical energy density, E_v^*, is ablated [3,22,25,49]. With an exponential decay of laser intensity given by Beer's law, the total number of molecules ejected per unit surface area is

$$N = n_{\mathrm{m}} L_{\mathrm{p}} \ln\left[\frac{F}{L_{\mathrm{p}}(E_v^* - CT_0)}\right], \qquad \text{for} \quad F \geq F_{\mathrm{th}} \tag{2}$$

where n_{m} is the molecular number density of the material, L_{p} is the laser penetration depth, C is a specific heat capacity of the model material, and CT_0 is the thermal energy density prior to laser irradiation. This expression predicts the existence of the threshold fluence $F_{\mathrm{th}} = L_{\mathrm{p}}(E_v^* - CT_0)$ at which the critical energy density E_v^* is reached in the surface layer. The solid lines in Fig. 1 are fits to Eq. (2).

Although the yield of ablated molecules for 150 and 15 ps laser pulses can be described by a volume ejection of material, the mechanisms responsible for the ablation onset are different in the two cases. For thermal confinement, there is a phase explosion or explosive boiling process. The phase explosion results in a decomposition of the expanding plume into a mixture of individual molecules and liquid clusters as shown in the snapshots in Fig. 1. The droplets are largest at fluences right above the threshold and decrease in size but increase in number as the fluence increases. The mass fraction of clusters/droplets in the ablation plume decreases from 91% at the ablation threshold of 37 J/m^2 to 75% at the maximum fluence simulated, 86 J/m^2. The corresponding decrease in the fraction of clusters/droplets in simulations performed in the stress confinement regime, with 15 ps pulse, is from 95% at the threshold (31 J/m^2) down to 77% at 86 J/m^2. The energetically efficient ablation in the stress confinement regime (15 ps pulse) is due to the contribution of the photomechanical effects caused by the relaxation of high laser-induced thermoelastic pressure. In this regime, at fluences just below the ablation threshold, we observe nucleation, growth, and collapse of voids underneath the surface, as shown in the snapshot in the lower left part of Fig. 1. As the fluence increases above the ablation threshold, the void growth and coalescence leads to the separation and ejection of large chunks of material, as discussed in Refs. [24,25,27] and shown in the snapshot in the lower right part of Fig. 1. The clusters ejected in the stress confinement regime are larger and more numerous as compared to the thermal confinement. At fluences close to the threshold value, the whole surface layer is separated and ejected. In these cases, the lateral size of the ejected chunks of the material is larger than the size of the largest computational cell used in the simulations, 40 nm. A detailed analysis of the dynamics of the cluster formation, their size

Fig. 1. Total yield as a function of laser fluence for simulations performed in the regimes of thermal confinement (●) and stress confinement (▲). The solid lines represent prediction of the ablation model, Eq. (2), with $E_v^* = 0.6$ eV for the thermal confinement and $E_v^* = 0.49$ eV for the stress confinement data. The dashed lines represent fits of the data points below the ablation threshold to the thermal desorption model, Eq. (1) with $E_{\mathrm{s}} = 0.46$ eV for both graphs. Included are snapshots from the simulations for thermal confinement just above the ablation threshold (39 J/m^2) and at 1.75 times threshold (61 J/m^2), and for stress confinement in the desorption regime (28 J/m^2) and just above the ablation threshold (31 J/m^2). The plume for desorption in the thermal confinement regime has mostly individual molecules similar to the stress confinement regime but there is no void formation in the sample. The frames at the top show the results from trapping plate experiments by Handschuh et al. [52] for fluences of 20, 40, and 120 J/m^2, from left to right. No clusters or analyte molecules are detected at 20 J/m^2, whereas molecular films of 1 and ∼20 nm thickness speckled with clusters are found to cover the trapping plate at 40 and 120 J/m^2, respectively. Simulation data are from Ref. [25].

distributions, and spatial distribution in the expanding plume is given in Refs. [50,51].

3.1.3. Experimental evidence of cluster ejection

Recent results from trapping plate experiments by Handschuh et al. performed under UV-MALDI conditions [52] provide a direct visual confirmation of the predictions of the model regarding the plume composition. The fluence dependence of the ejection of small submicron sized particles observed in Ref. [52] is shown at the top of Fig. 1. No particle ejection is observed below the ablation threshold. Right above the ablation threshold there is the appearance of particles. As the fluence is increased, the number of particles increases and the size of the particles decreases, consistent with the simulations. Simulation results for the stress confinement regime suggest that larger clusters should be observed in IR-MALDI.

Indirect evidence of the ejection of molecular clusters in MALDI has been obtained in postionization time-of-flight MS experiments by Hankin and John [53]. A nonlinear dependence of the time-of-flight from the delay time in the delayed extraction experiments observed by Fournier et al. have been explained by a delayed ion formation from higher mass precursors [54]. Recent investigation by Krutchinsky and Chait suggests that clusters of matrix molecules are largely responsible for the "chemical noise background" in MALDI mass spectra [55]. It has been also proposed that molecular clusters [56–58] play a key role in the MALDI ionization process. Besides MALDI, the ejection of liquid and/or solid particulates in laser ablation has been observed for a wide range of target materials and appears to be a rather general phenomenon [59–62].

3.1.4. The effect of volatility: simulation and experiment

The prediction from the simulations that the low-fluence regime of molecular ejection is characterized by a process of thermal desorption from the surface and the high-fluence regime by a volume-ejection process has been verified in a joint experimental–computational study [26]. Experimental studies were performed with several small analyte molecules, e.g., decane and dimethylether, in a matrix of toluene. Electron impact ionization was used in order to detect both the neutral matrix and analyte molecules. Analogous calculations were performed with analyte molecules that were less volatile ("nonvolatile") and more volatile than the matrix molecules. Shown in Fig. 2 are the compositions of the plume vs. laser fluence from the experiments and simulations. The concentrations have been normalized to the initial concentrations of analyte molecules in the original samples and the fluences have been normalized to the threshold fluences. The results clearly show that in the desorption regime the volatility of the analyte molecules is the major factor that defines their presence in the plume. In both the experiments and the

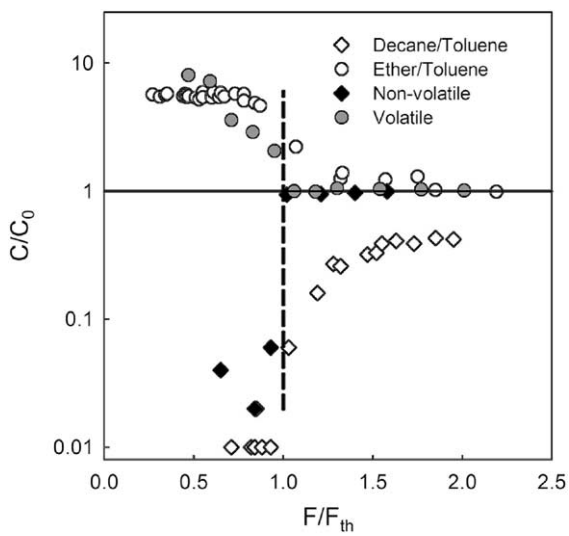

Fig. 2. Concentration of small analyte molecules in the plume as a function of laser fluence from mass spectrometry measurements (○,◇) and MD simulations (●, ◆). The concentration of the analyte molecules is scaled to the initial concentration, C_0, and the fluence is scaled to the threshold fluence, F_{th}. The symbols correspond to: (●)—experimental data for dimethyl ether/toluene system, $C_0 = 16.7\%$, $F_{th} = 120\,mJ/cm^2$; (◆)—simulations with volatile analytes, $C_0 = 10\%$, $F_{th} = 35.3\,J/m^2$; (◇)—experimental data for decane/toluene, $C_0 = 16.7\%$, $F_{th} = 175\,mJ/cm^2$; (◆)—simulations with nonvolatile analytes, $C_0 = 10\%$, $F_{th} = 44.8\,J/m^2$. The dashed vertical line corresponds to the ablation threshold fluence. The original experimental data and calculated results are from Ref. [26].

simulations at low laser fluences, the volatile species (ether) dominates the plume whereas the nonvolatile speces (decane) is present, at most, in trace amounts. This result confirms that the physics of molecular ejection is the thermal desorption from the surface. Above the ablation threshold where the simulations predict a volume-ejection process, the concentration of analyte in the plume matches the initial concentration in the sample. The slightly lower concentration of the decane above the ablation threshold, as compared to the initial concentration, has been interpreted to be due to the preferential incorporation of decane molecules in clusters that are not as easily detected [26]. Although the experimental data and the results from the calculations shown in Fig. 2 appear to be in good agreement, the interpretation of the conventional MALDI data on ion signals is not as straightforward.

3.1.5. MALDI yields

An example of experimental ion yields vs. laser fluence is shown in Fig. 3 for bovine insulin in a matrix of sinapic acid [8]. The signals of the protonated insulin ions, the matrix ions, and the neutral matrix molecules postionized by a second laser are measured. The yield vs. fluence curves do not exhibit an obvious ablation threshold. Rather, the experimentalists contend that only detection thresholds exist. How does one, then, correlate these results with the calculations? It is important to note that the neutral matrix molecules are observed at lower laser fluences than the matrix and insulin ions.

The experimental measurements are for individual molecules or monomers. The yields shown in Fig. 1, on the other hand, contain a considerable contribution from clusters and liquid droplets. Shown in Fig. 3 is the calculated monomer yield as a function of fluence. The most striking feature is that the ablation threshold is not apparent in the calculated monomer yield. Computational results show that neutral matrix molecules can desorb from the surface at low fluences. These molecules can be detected in the postionization experiments. The volume ejection or ablation is needed for

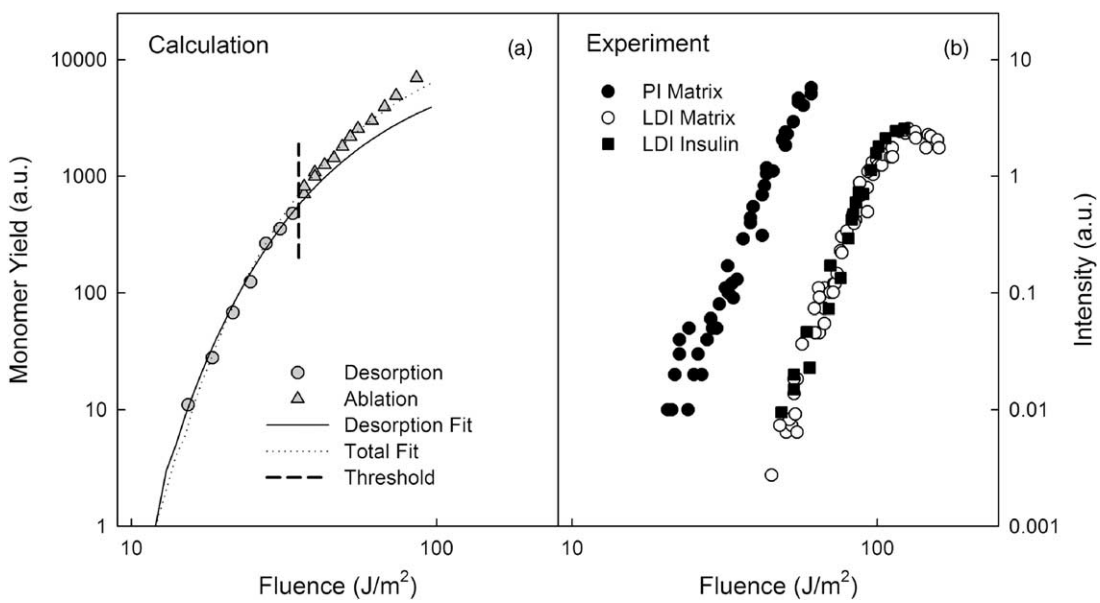

Fig. 3. Yield of monomers in simulations and MALDI experimental data. The calculated monomer yields are from the simulations performed with 150 ps laser pulse, the lines are fits to Eq. (1). The dashed vertical line denotes the ablation threshold. The experimental data for insulin in sinapic acid are identical to the values in Fig. 9 of Ref. [8]. The natural laser desorption ions (LDI) are detected for both the matrix molecules and the protonated analyte molecule. Postionization (PI) experiments were done to detect the neutral matrix molecules. The original data from the simulations is in Ref. [25].

the ejection of the insulin molecules (and ions). The ablation threshold in the experimental system is thus near the onset of the detection of analyte molecules and ions.

The experimental data in Fig. 3 are found to best fit the Arrhenius equation for thermally activated desorption, Eq. (1) [8]. The authors go on to question whether, in fact, this model contains the correct physics for the ablation process. Shown in Fig. 3 are two fits of Eq. (1) to the calculated monomer yield. The solid line corresponds to a fit to the data points only in the desorption regime where it is applicable. The other fit is to both the desorption and ablation regimes. It is clear from the simulations that a volume ejection of material is occurring in the ablation regime and that Eq. (1) should *not* be applicable, but the fit in Fig. 3 to the monomer yield appears to be excellent. The apparent fit is thus misleading in terms of the actual physics underlying the molecular ejection.

Finally, a mention of the comparison of absolute fluences should be made. There are several differences between the values used in the simulations and the real parameters of the sinapic acid matrix. First, the heat capacities of the molecules in the two systems are different. The model system only has one internal degree of freedom whereas a real molecule has considerably more vibrational degrees of freedom. Second, we assume no reflection losses in the simulation. Third, we assume that all of the laser energy is potentially available for heating the matrix. All these approximations reduce our threshold fluences as compared to the experimental values. On the other hand, the laser penetration depth of 50 nm, used in the simulations, is about twice shorter than the one measured for sinapic acid at 337 nm [39]. The lower penetration depth decreases the threshold fluence needed for the ablation onset. Quantitative estimates of the corrections are given in Refs. [22,26].

3.2. Analyte molecules

A big question with MALDI is how the large analyte molecules lift off the surface without fragmenting, escape solvation by the matrix molecules and ultimately reach the detector. Two types of computational models are being used to study these issues with different resolutions—conventional atomistic MD models [11–15] and the mesoscopic breathing sphere model [16,19,20,26,63,64]. The strength of the atomistic MD simulations is that the internal vibrational motions are explicitly incorporated (at least classically) and energy redistribution between the internal and translational degrees of freedom of matrix and analyte molecules can be studied. The weakness of the atomistic MD simulation is that the technique is computationally expensive and only small systems can be investigated for relatively short times. These limitations make it difficult if not impossible at all to incorporate irradiation parameters, such as pulse width, laser fluence, and Beer's law absorption into the simulations. On the other hand, the irradiation parameters can be incorporated into the mesoscopic breathing sphere model and relatively large systems can be simulated. The transfer of the internal vibrational energy from the matrix molecules to the analyte molecule, however, cannot be investigated.

In our opinion, there are still open questions about the ejection conditions that analyte molecules experience during the ablation, character of their interaction with other species in the plume, and the final characteristics of the analyte molecules at the time when they reach the detector. Below we give a summary of what questions we feel have been answered and which ones remain.

3.2.1. Lift off of molecules

Depositing energy into the matrix causes the analyte molecules to be lifted off the surface in atomistic [11–13,15], breathing sphere [16,19,20,26], or bead-and-spring [63,64] representations of the analyte molecule. Shown in Fig. 4 is the time evolution of a bead-and-spring representation of an analyte molecule of mass 11 kDa. Clearly the molecule has been lifted off as a result of the entrainment into the expanding plume of matrix molecules. Both the atomistic [12,14] and mesoscopic breathing sphere [26,64] simulations show that the large analyte molecules only eject above the ablation threshold. In the desorption regime, only

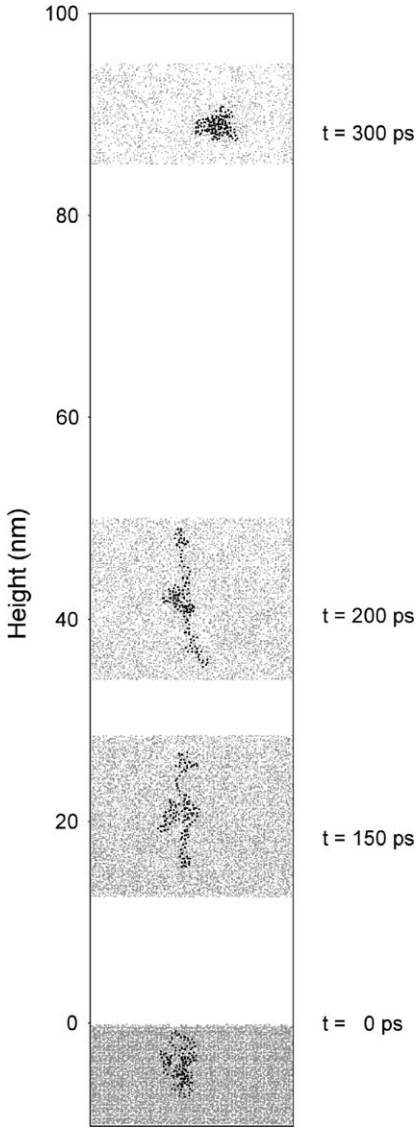

Fig. 4. Time snapshots of portions of the plume for the ablation of 11 kDa analyte molecule (150 beads of 74 Da each). Only the portions of the plume near the analyte molecule at each time snapshot are shown. The matrix molecules are gray dots and the beads in the analyte molecule are black dots. The laser pulse duration is 150 ps, laser penetration depth is 40 nm, and the fluence is 70 J/m^2. The time is defined relative to the start of the laser pulse.

the matrix molecules depart from the surface. This result is consistent with the experimental results shown in Figs. 2 and 3.

3.2.2. *Velocities of analyte molecules*

There have been several measurements of the velocity of the analyte ions [9,65–72]. The measured axial velocities are in the hundreds of meters per second range, comparable to the velocities of the matrix molecules. Definitive correlations of the velocities of the analyte molecules with their mass and the choice of the matrix substance have not as yet been identified. In early delayed extraction experiments, Beavis and Chait [9] observed similar initial velocity distributions for analyte ions of different masses, from 1000 to 15,600 Da. There was, however, an appreciable difference in the most probable velocities of matrix and analyte molecules. No substantial difference between velocities of matrix and analyte ions was observed by Pan and Cotter [68]. Nearly identical velocity distributions were also measured by Huth-Fehre and Becker [66] for postionized neutral matrix and analyte molecules, although the matrix distributions have a tail that extends to higher velocities than the analyte distribution. The mass-independent velocity distributions have been attributed to the entrainment of the analyte molecules in the expanding matrix plume [9,66].

More recent and comprehensive investigations [67,70] revealed a strong dependence of the initial velocities of ions in MALDI on the type of matrix and analyte, sample preparation protocol, and the degree of incorporation of the analyte into matrix, as well as on the presence of additives to matrices. Although the dependence of the initial velocities of MALDI ions on numerous factors complicates the analysis, it also indicates that the ejection velocity of ions can be regarded as a useful characteristic of MALDI sensitive to the mechanisms of ejection and ion formation [70]. Finally, in a recent paper by Berkenkamp et al. [72], the initial velocities of analyte and matrix ions are measured in IR- and UV-MALDI using different ion extraction technique. Substantially higher initial velocities of IR-MALDI ions are typically obtained by the free-field drift method as compared to the delayed

extraction method. The energy deficit observed for short delay times in the delayed extraction experiments is largely attributed to the collisional deceleration of the ions extracted from the dense neutral plume.

On the computational side, we have performed initial simulations aimed at understanding of the dependence of the velocity distributions on irradiation conditions and incorporation into the matrix. To study the laser fluence dependence of the ejection velocity we used a model with a bead-and-spring representation of the analyte molecules [64]. The final velocity of a molecule with mass of 7.4 kDa (100 beads of 74 amu each) initially located near the surface of the sample is shown as a function of laser fluence in Fig. 5a. We find that there is a strong dependence of the velocity on the laser fluence. Near threshold, the velocity is lowest and it increases with fluence and thrust of the phase explosion.

In our earlier simulations aimed at understanding the mass dependence of the velocity distributions we used the breathing sphere representation of the analyte molecules [19,20]. We found that the ejection of the analyte molecules is driven by the relaxation of the laser-induced pressure and the explosive decomposition and ejection of a surface region of the sample. The analyte molecules are entrained into expanding plume of matrix molecules and clusters and their velocities exhibit only a weak dependence on molecular mass. A much stronger dependence has been observed in recent simulation with a bead-and-spring representation of the analyte molecules. In these simulations the analyte molecules are initially located in the very surface region of the sample irradiated at a fluence of 70 J/m^2, a value about twice the ablation threshold. The mass dependence of the final velocities of the analytes is shown in Fig. 5b. This strong mass dependence can be partially attributed to the relatively shallow laser penetration depth of 40 nm and a small size of the computational cell used in the simulations. The extension of the analyte molecule along the plume flow direction, as observed in Fig. 4, can reduce the collision cross section of the molecules in this direction and decrease the efficiency of entrainment and the final velocity of the analytes. This effect of "straggling" of analyte molecules in the plume, proposed by Beavis and Chait [9] to explain the difference in velocities of matrix and polypeptide ions, can also contribute to the mass dependence observed in the simulations. A more systematic investigation of the mass dependence of the ejection velocities of the analyte molecules and their dependence on the laser penetration depth, geometrical parameters of the analyte molecules (e.g., linear

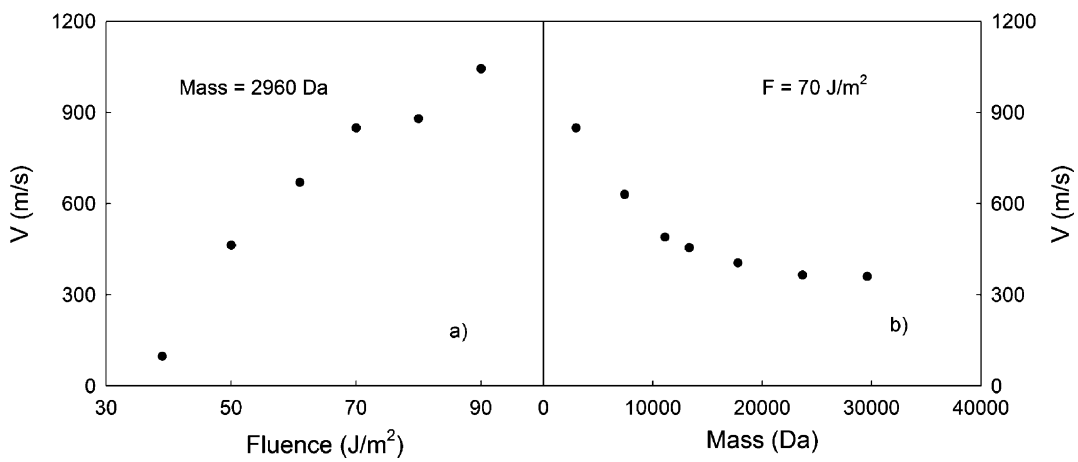

Fig. 5. Calculated velocity of an analyte molecule as a function of laser fluence and mass. For all the simulations the analyte molecule is initially located right under the surface, similar to the configuration shown in Fig. 4. The laser pulse duration is 150 ps and the laser penetration depth is 40 nm. (a) Velocity vs. fluence for a mass of 2960 Da. (b) Velocity vs. mass for a fluence of 70 J/m^2.

vs. globular structure), initial position of the molecule in the sample, and strength of matrix–analyte interaction is being currently investigated.

The calculations show that in addition to mass and fluence, the final velocities of the analyte molecules have a strong dependence on the initial depth of the molecule under the surface [13,15,19,20,63,64]. Namely, the molecules nearest to the surface have, on average, higher velocities than molecules initially deeper in the matrix. Thus, the values shown in Fig. 5 for a molecule near the surface are larger than the velocities of molecules initially deeper in the matrix. In addition, the fluences used for different systems must be correlated to the respective ablation thresholds and properties of the matrix. Finally, it is unknown how the ionization probability of the ablated molecules depends on their original position in the sample and other parameters discussed earlier. It is not surprising that clear trends have not been identified in the experimental data. The discussion of the velocity and angular distributions of ejected molecules and their dependence on the irradiation conditions is given in Section 3.3.

3.2.3. Motion and desolvation of analyte molecules

The analyte motion during the ablation process is shown in Fig. 4. The analyte molecule initially extends itself and then re-agglomerates. Moreover, there are numerous matrix molecules surrounding the analyte molecule. Clearly, any original conformation of the analyte molecule is lost in the simulations. Moreover, during the course of the phase explosion and plume evolution, internal sites of the analyte molecule are exposed to the surrounding species in the cluster and in the plume, providing more possibilities for the ionization reactions. The conformational changes of the analyte molecule during the ejection process have been observed in a number of atomistic [11,13,15,73] and breathing sphere [64] simulations. Certainly, the stability of the native conformation during the ablation process depends on many factors including irradiation conditions and the details of inter and intramolecular interactions and more systematic and detailed analysis is needed to address this issue.

Both the breathing sphere [64] and atomistic [15] simulations predict that the ejected analyte molecules are typically incorporated into clusters of matrix molecules. Furthermore, the breathing sphere simulations show that the number of matrix molecules in the clusters decreases with time, although we can only follow the plume for about 1 ns. The simulations also predict that the number of matrix molecules attached to the analyte molecule decreases with increasing fluence and is least for molecules initially near the surface.

Although some experiments show that analyte molecules can be detected as a part of high mass cluster ions [74,75], in general, MALDI spectra do not exhibit peaks associated with solvated analyte ions. We have discussed possible mechanisms for desolvation [64] including the thermal evaporation of clusters during the tens of microseconds it takes for the molecule to reach the detector and the gas-phase collisions during the cluster ion extraction. In general, we have not reach a definitive conclusion. We are convinced, however, that many of the ejected analyte molecules are initially incorporated into clusters of matrix molecules and are desolvated later during the plume development. Fournier et al. [54] proposed that acceleration by the applied electric field desolvates the molecule. Russell and co-workers propose that the desolvated analyte molecules are originally on the surface [76], a configuration we have not as yet investigated.

3.3. Velocity and angular distributions

The experimental velocity and angular distributions exhibit clear trends. The most distinctive signature of the distributions is that the axial velocities are much larger and have a broader distribution as compared to the radial velocities [10,65,69,77,78]. Consequently, the angular distributions are strongly forward peaked. Moreover, the angular distributions of the analyte molecules are even more forward peaked than the ones of the matrix molecules [68].

The breathing sphere MD simulations provide sufficient statistics to examine complete velocity and angular distributions of the molecules ejected in a simulation. In previous investigations [18–20,25] we

have shown that the axial velocity distribution can be characterized by a modified Maxwell–Boltzmann distribution with a *range* of stream velocities [18,20] and that the radial distribution can be described by an ordinary Maxwell–Boltzmann distribution with the same temperatures used in both distributions. This results in a strong forward peaking of the angular distributions.

The analyte molecules are entrained into the expanding plume of matrix molecules, Fig. 4, and are moving at nearly the same axial velocities as the matrix molecules. For the analytes, therefore, the spread in the axial velocities is due to the entrainment into different parts of the expanding plume, has only a weak mass dependence, and is not significantly affected by the thermal motion [20]. At the same time, the radial velocity distributions are due to the thermal motion and become narrower with increasing molecular mass. Thus, while both matrix and analyte molecules have forward-peaked angular distributions, the analyte molecules of higher masses (analytes of three different masses, 2, 4, and 10 kDa were introduced in the simulations) exhibit a higher degree of forward peaking [20].

The forwarded ejection discussed earlier can be illustrated by angle–velocity distributions shown in Fig. 6a–c for matrix monomers ejected in simulations

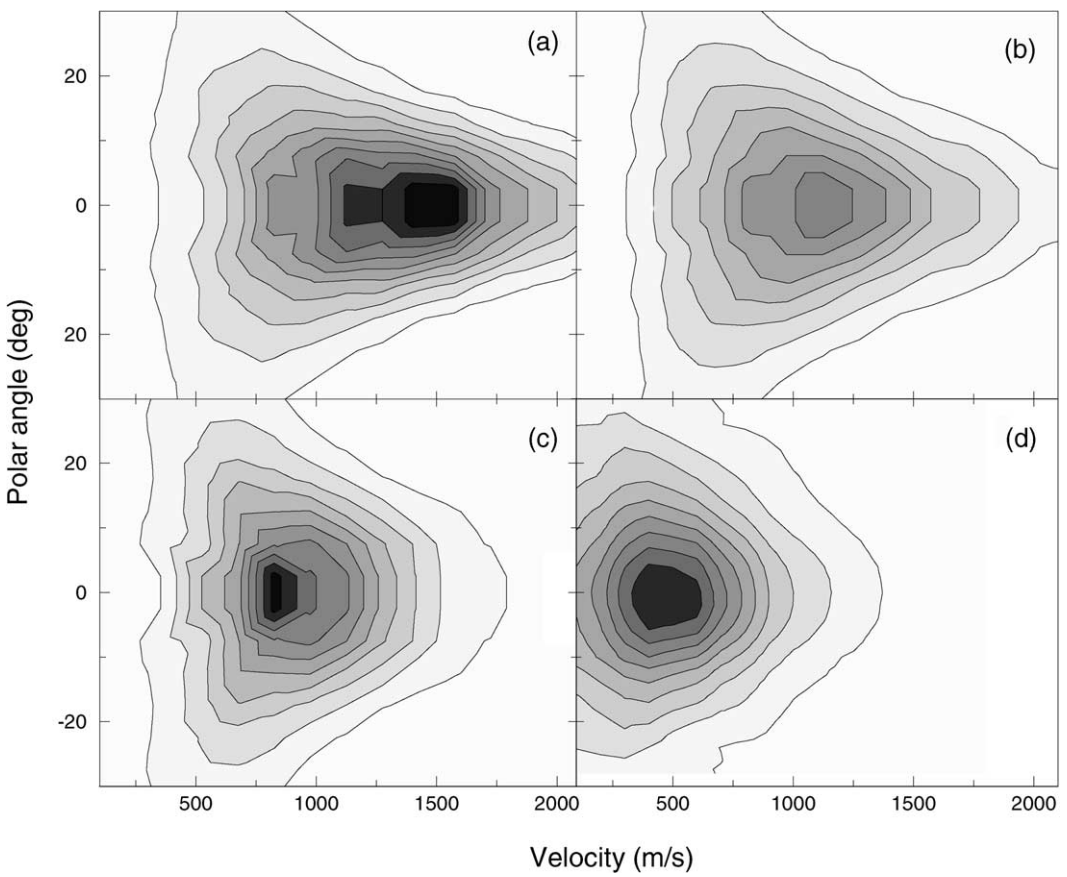

Fig. 6. Contour plots of angle–velocity distributions of the ejected matrix monomers in simulations and experiment: (a) simulation with 61 J/m^2, 15 ps pulse; (b) simulation with 61 J/m^2, 150 ps pulse; (c) simulation with 39 J/m^2, 15 ps pulse; and (d) experimental data from Ref. [77] for postionized molecules ejected in laser ablation of Trp-Gly. In simulations, (a–c), the density of the molecules per solid angle is normalized to the total number of ejected molecules. The experimental data in (d) is normalized to the maximum of the distribution.

performed for the 15 ps laser pulse at 39 and 61 J/m^2 and for the 150 ps laser pulse at 61 J/m^2. The density of the ejected molecules per solid angle is normalized in these plots to the total number of ejected molecules. For comparison purposes, we also show in Fig. 6d an experimental angle–velocity distribution of laser-ablated Trp-Gly measured by Elam and Levy [77]. In this experiment, that is configured [79] similarly to the one used in kilo electron volt particle bombardment studies [80], the ejected molecules are postionized with a second laser and detected using a time-of-flight multichannel plate detection scheme. The data are normalized in this case to the maximum of the distribution and the levels of the experimental contour plot in Fig. 6d do not match the ones in Fig. 6a–c. Several points can be made based on the results shown in Fig. 6.

1. All the distributions are strongly forward peaked–the intensity decreases by an order of magnitude as the polar angle increases beyond 30°.
2. The distribution has a stronger forward peaking and is shifted to the higher velocities in the regime of stress confinement as compared to the thermal confinement. The intensity of the peak is 25% lower in Fig. 6b as compared to Fig. 6a, and the respective peak positions are 1125 and 1425 m/s.
3. The ejection velocities decrease significantly as the fluence decreases from 2.1 times the threshold fluence, Fig. 6a, to 1.34 times the threshold fluence, Fig. 6c, but the distribution remains strongly forward peaked.
4. There is a good qualitative agreement between the simulation results, Fig. 6a–c, and the experimental distribution, Fig. 6d. A quantitative comparison is difficult due to the sensitivity of the peak positions to the irradiation conditions, properties of the matrix, and the detection technique.

3.4. Pressure waves

Piezoelectric detection of pressure waves generated by pulsed laser irradiation provides an attractive opportunity to obtain information on the laser-induced processes in the absorption region complementary to the mass spectrometry measurements. Experimental observations indicate that the shape and the amplitudes of the pressure wave have a strong dependence on the irradiation conditions [44,49,81–86], although the direct links between the results of photoacoustic measurements and complex processes in the absorption region still have to be established. In this section we take advantage of a comprehensive picture of the laser-induced processes provided by the MD simulations and perform a detailed analysis of the relations between the character of the molecular ejection in the regimes of thermal and stress confinement and the parameters of the pressure waves. We then relate the simulation results to the results of recent photoacoustic measurements performed for IR-MALDI by Dreisewerd et al. [86].

Temporal pressure profiles produced in the sample by pulsed laser irradiation can be monitored in the calculations [23,25] and measured experimentally [44,86]. The pressure profiles generated at low, below the ablation threshold, fluences exhibit a characteristic bipolar shape that results from the interaction of the laser-induced compressive thermoelastic pressure with free surface of the irradiated sample [23]. Specific predictions about the nature of the compressive and tensile components of the bipolar wave arise from the simulations. A detailed discussion is given in Ref. [25], thus we only give the highlights of results here.

- The pressure signals are strongest in the stress confinement regime and decrease significantly as the irradiation conditions shift out of stress confinement, e.g., due to the increase of the laser pulse width or decrease of the laser penetration depth.
- The amplitude of both the compressive and tensile components of the pressure wave increase linearly with fluence in the desorption regime.
- Above the ablation threshold, the strength of the compressive signal continues to increase nearly linearly.
- Above the ablation threshold, the amplitude of the tensile component saturates and decreases with increasing fluence. The decrease is more pronounced in the stress confinement regime.

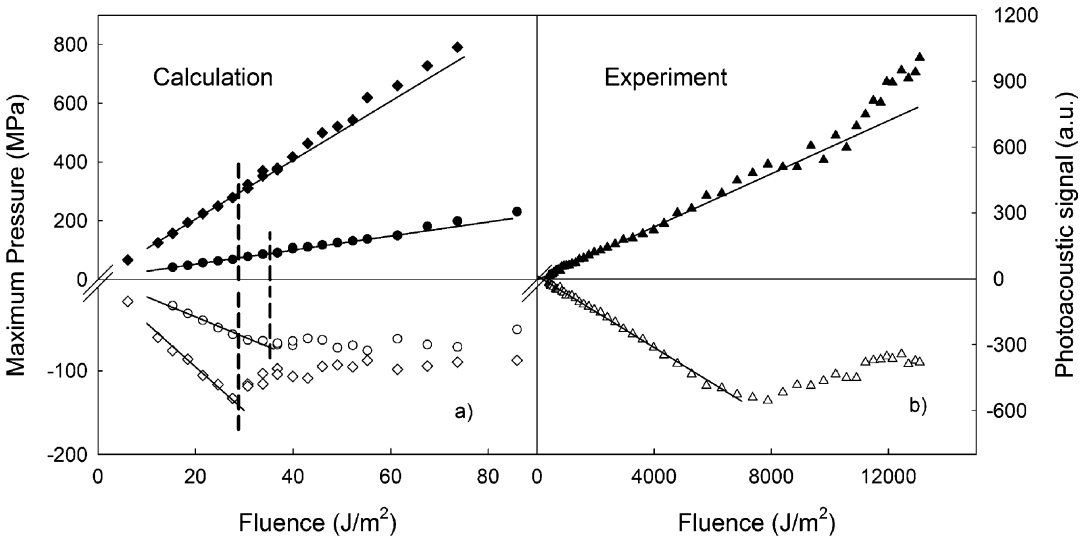

Fig. 7. Amplitudes of the compressive and tensile components of the laser-induced pressure wave as a function of laser fluence. Compressive components are positive and represented by solid symbols. Tensile components are negative and represented by open symbols. The solid lines are the linear fits to the data points in the desorption regimes. The dashed vertical lines denote the ablation thresholds in the calculations. (a) Calculations from Ref. [25]. The symbols correspond to: (◆, ◇)—calculations with 15 ps laser pulse, (●, ○)—calculations with 150 ps laser pulse. (b) IR-MALDI experiments for glycerol matrix irradiated with 6 ns pulse at 2.94 μm, [86].

The observations summarized are illustrated in Fig. 7, where the amplitudes of the compressive and tensile components of the laser-induced pressure waves are shown as a function of laser fluence for the simulations performed with the 15 and 150 ps laser pulses. In the simulations, the depth of the pressure recording is limited by the size of the computational cell and is only 100 nm under the irradiated surface. At this depth the direct laser energy absorption contributes to the buildup of the compressive pressure during the laser pulse and artificially adds to the positive component of the pressure profile [23]. Consequently, we have different scales for the compressive and tensile pressures in Fig. 7.

Examining first the results for the 15 ps laser pulse, that are clearly in the stress confinement regime, we observe a near linear increase in the compressive pressure with fluence. Some deviation from the linear dependence observed at high fluences can be attributed to the contribution of the compressive recoil pressure imparted by the massive material ejection in the ablation regime. The tensile pressure, on the other hand, linearly increases in magnitude until the ablation threshold at which point there is a sharp break. As the fluence increases in the ablation regime, the tensile pressure decreases slightly in magnitude. The results from the calculations for the 150 ps laser pulse are qualitatively similar to the 15 ps results but the magnitudes of the pressure signals are smaller. The most notable difference is that the sharp break in the tensile pressure at the ablation threshold for the 15 ps simulations is now a gradual change for the 150 ps simulations.

The difference between the tensile components of the pressure wave for the 15 and 150 ps calculations can be related to the difference in the processes responsible for the ablation onset in the stress and thermal confinement regimes, as discussed in Section 3.1. For the 15 ps pulse, the sharp break in the fluence dependence of the amplitude of the tensile pressure corresponds to the onset of the laser-induced spallation of the surface layer, and the observed maximum amplitude of the tensile stresses corresponds to the dynamic tensile strength of the material, weakened by

the laser heating [24,25,27]. In the case of 150 ps pulse in the regime of thermal confinement, the amplitude of the laser-induced tensile stresses is smaller and photomechanical effects do not play any significant part in material ejection. For 15 ps laser pulses in the regime of stress confinement, a significant decrease of the amplitude of the tensile component of the pressure wave at high laser fluences can be explained by contribution of the following two processes. First, the effect of thermal softening can significantly reduce the dynamic tensile strength of the material in the surface region of the sample at higher laser fluences, limiting the ability of the material to support the tensile stresses. Second, the tensile stresses produced by the thermoelastic mechanism can be obscured in the ablation regime by superposition with the compressive recoil pressure from the ejection of the ablation plume.

The dependence of the compressive and tensile pressure on laser fluence has recently been investigated in IR-MALDI experiments with 6 ns laser pulse at 2.94 μm and glycerol as an MALDI matrix [86]. The experimental data are shown in Fig. 7. The general appearance of the experimental curves is similar to the calculated curves.

As discussed in Sections 2.3 and 3.1, in general, irradiation conditions in IR-MALDI correspond to the stress confinement regime and thus the experimental curves should be comparable to the calculated ones with the 15 ps laser pulse. There is no sharp break in the dependence of the tensile photoacoustic signal, however, suggesting that the experiments are not completely in the stress confinement regime. Indeed, using the decadic molar extinction coefficient of 175 L/mol/cm given for glycerol matrix at 2.94 μm in Ref. [87], we can estimate that the ratio of the pulse duration to the characteristic time of the relaxation of the laser-induced thermoelastic stresses ($\tau_s \sim L_p/C_s$, where C_s is the speed of sound in the irradiated material and L_p is the laser penetration depth) is 6.8, close to the one in the simulations performed with 150 ps laser pulse. The decrease of the tensile photoacoustic signal in the experiment can be associated, therefore, with contribution of the ablation recoil pressure rather than spallation and thermal softening discussed earlier. Moreover, a gradual deviation from the linear dependence characteristic for the thermal confinement regime makes it difficult to clearly identify the ablation threshold from the photoacoustic data. Note that under typical UV-MALDI condition (e.g., $L_p = 200$ nm, $\tau_p = 3$ ns) the ratio $\tau_p/\tau_s \approx 30$, a much larger value than in the simulations and experiment discussed earlier. In this case any detectable thermoelastic signal is unlikely to be generated.

Both experimental measurements and the results of the present simulation study suggest that the shape and parameters of the acoustic wave propagating from the absorption region are sensitive to the changes in the mechanisms of material ejection and can be used for tuning of the irradiation parameters to the desired ejection conditions. Simulations allow us to directly relate the characteristics of the pressure waves to the molecular-level picture of laser desorption, ablation, and damage and can help in interpretation of experimental data from photoacoustic measurements.

3.5. Spatially localized absorbers

The ability to investigate inhomogeneous systems and different geometries was one of the original objectives in designing the mesoscopic breathing sphere model. One of the projects in which we take advantage of the flexibility of the model is the computational investigation of the mechanisms of disintegration of submicron molecular particles [88–91]. Small, spatially localized absorbers are used in a number of laser irradiation applications. An example from laser surgery is the strong absorption of visible and near IR radiation by melanin granules, submicron pigment particles naturally occurring in many tissues including skin and eye retina [92–95]. In laser ablation of polymers, absorption within nanometer-sized inclusions of graphite reduces the threshold for short-pulse ablation [96]. As a basis for the analysis of mechanisms of laser ablation in these complex systems, the knowledge of the effect of laser irradiation on an isolated or embedded particle is essential. The understanding of the mechanisms of laser ablation of individual particles is also critical for interpretation of data

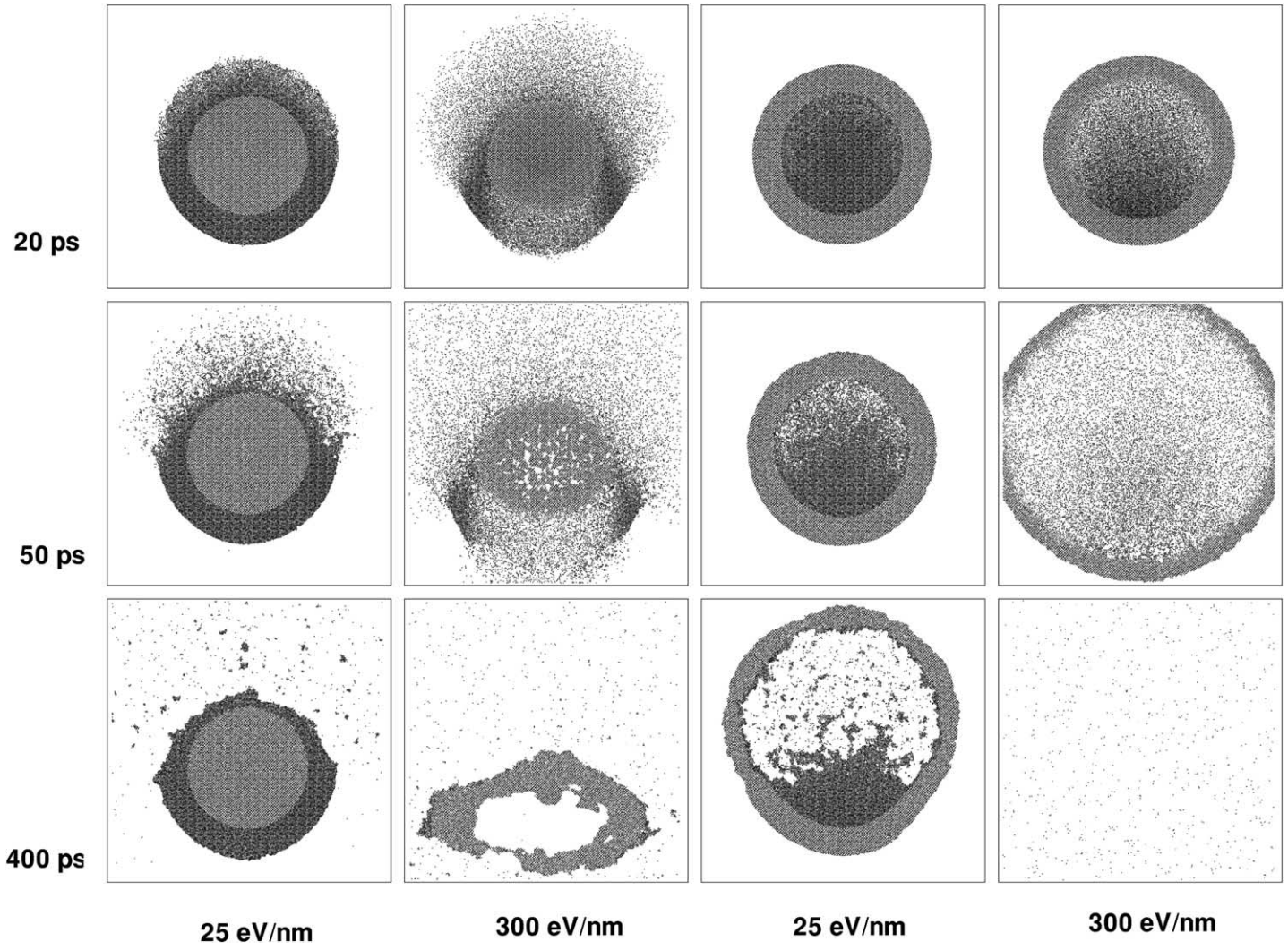

Fig. 8. Snapshots from simulations of two-dimensional amorphous particles containing inclusions. Either the inclusion or surrounding material absorbs laser irradiation. Black parts of the particles correspond to the absorbing material whereas gray parts are transparent to the laser light. The diameters of the inclusion material and the overall particle are 66 and 110 nm, respectively. Particles are irradiated with a 15 ps laser pulse. The laser originates from the top of the figure and the absorption profile follows Beer's Law with laser penetration depth of 25 nm. Two laser fluences are used, 25 and 300 eV/nm. Snapshots are shown for times 20, 50, and 400 ps after the start of the laser pulse. Since the simulations were performed in two-dimension, the units of fluence are electron volts per nanometer.

from real-time aerosol characterization experiments [97–99].

For the initial investigation we have chosen to use a two-dimensional version of the breathing sphere model as it offers a clear visual picture of laser-induced processes and gives the same qualitative results as the three-dimensional model in considerably shorter computer time [90,91]. Fig. 8 shows various scenarios of laser-induced disintegration of a heterogeneous particle with an inclusion. We have assumed that either the inclusion or surrounding material absorbs the laser irradiation. One hundred percent dissociation of the particles does not occur regardless of laser fluence or particle composition. At low laser fluences, we observe the ejection of a certain amount of absorbing material if it is the coating, and none if it is the inclusion. When the laser fluence is sufficiently high, both the absorbing and the transparent material are sampled, with the transparent material making up a smaller fraction of the ejected molecules. The ability to sample a transparent material by coating it with an absorbing material has been recently demonstrated experimentally for atmospheric ammonium sulfate aerosols [100]. Ammonium sulfate particles are difficult to detect by laser desorption ionization (LDI) in real-time single-particle mass spectrometry because it is a poor absorber at most of the wavelengths used in LDI. By coating ammonium sulfate particles with ∼12 nm of 1-napthyl acetate, Kane and Johnston have been able to increase the yield of ammonium sulfate particles by a factor of 20 using a 193 nm wavelength. How the thickness of the coating affects the amount of ejected transparent material is being investigated.

3.6. Photochemical effects

The analyte molecules typically used in MALDI are selected because of their transparency to the UV laser irradiation. In fact, before MALDI was invented by Karas and Hillenkamp [1], researchers were attempting to directly irradiate a sample composed of molecules of interest in order to induce desorption of the molecules to be mass analyzed [101]. Although mass spectra sometimes could be obtained, there was a deleterious side effect of fragmentation of the molecules, i.e., photochemistry was occurring. In other situations, photochemistry is a desired effect, for example, ablative photodecomposition of polymers and biological tissue [49] is used for etching the holes in polyimide in ink jet printers and in the corrective vision surgery, LASIK techniques [102].

In order to understand the role of photochemistry in the ablation process we have developed and implemented a strategy for incorporating the photochemical processes into the breathing sphere model [36,37]. The excited molecule in the model can break into radicals, which then subsequently undergo abstraction and recombination reactions. We have chosen chlorobenzene as our basic system to model photochemical events because of its well-known gas-phase and solution chemistry. Photofragmentation of chlorobenzene entails exclusively scission of the C–Cl bond to yield C_6H_5 and Cl radicals, which in solution and static gas cell experiments react with the precursor molecule to form a number of different products. One major effect of the photochemical reactions is to drastically alter the amount and spatial distribution of the energy available for the events associated with ablation. At the beginning of the laser pulse part of the photon energy goes to bond scission and is thus not available to heat the sample. As time progresses, the number of radicals increase. In addition, the temperature rises and the radical mobility increases. Subsequent radical abstraction and recombination reactions give off heat that is available to further increase the temperature and pressure of the sample. The ramifications of the changes in energy and composition on the sample have been discussed [36,37] and are still under investigation.

4. Conclusions

While MD simulations have provided insights into many aspects of the desorption/ablation phenomenon and contributed to the recent progress in fundamental understanding of the processes involved in MALDI, many questions still await further investigation. In particular, there are issues associated with the ejection

of analyte molecules that we understand and some that we do not. We believe that our simulations show definitively that the analyte molecules only eject in the ablation regime, and that we can predict sensible values of their ejection velocities. In addition, we believe that the ejected analyte molecules are initially incorporated into clusters of matrix molecules. The unresolved issues include the analyte desolvation mechanisms, the amount of energy transferred to the internal molecular vibrations during the ejection and desolvation, the role of thermal and mechanical effects in fragmentation of the analytes under different irradiation conditions. The dependence of the ejection velocities of analyte molecules on irradiation conditions, laser penetration depth, mass, initial conformation of the analyte molecule in the matrix, depth of origin, strength of matrix–analyte interactions also still await a systematic investigation. Finally, the key issue in MALDI that has not been addressed in MD simulations so far is ionization. We believe that further computational studies have a potential to address the unresolved questions and to contribute to our understanding of MALDI and advancement of this important analytical technique.

Acknowledgements

We are honored to have been asked to write an article for this special issue of IJMS in honor of Franz Hillenkamp. Over the past 5 years that we have been developing this model, Franz has both asked hard questions about the model and simultaneously encouraged us to bring it closer to the experimental conditions. We also appreciate the support of R. Srinivasan who in 1983 got us started modeling ablation and who in the past few years encouraged our new approach. Discussions and data for this article from Klaus Dreisewerd, Jeff Elam, Savas Georgiou, Don Levy, and Renato Zenobi are gratefully appreciated. In addition, we have had fruitful discussions with Michael Berns, Gerard Bolbach, Dana Dlott, Richard Haglund, Robert Johnson, Murray Johnston, Charles Lin, Richard Knochenmuss, Kim Prather, and Peter Williams. Of course, other group members have contributed to publications and discussions including Arnaud Delcorte, Yusheng Dou, Prasad Kodali, Julia Smirnova, Gareth Williams, Nicholas Winograd, and Michael Zeifman. We gratefully acknowledge financial support from the Medical Free Electron Program (initially from the Office of Naval Research and now the Air Force Office of Scientific Research) and the Chemistry Division of the National Science Foundation. The computational support for this work was provided by the IBM Selected University Research Program and the Center for Academic Computing at Penn State University.

References

[1] M. Karas, F. Hillenkamp, Anal. Chem. 60 (1988) 229.
[2] F. Hillenkamp, M. Karas, R.C. Beavis, B.T. Chait, Anal. Chem. 63 (1991) 1193A.
[3] R.E. Johnson, in: T. Baer, C.Y. Ng, I. Powis (Eds.), Large Ions: Their Vaporization, Detection and Structural Analysis, Wiley, New York, 1996, p. 49.
[4] R.E. Johnson, J. LeBeyec, Int. J. Mass Spectrom. Ion Processes 177 (1998) 111.
[5] A. Vertes, R. Gijbels, in: A. Vertes, R. Gijbels, F. Adams (Eds.), Laser Ionization Mass Analysis, Wiley, New York, 1993, p. 127.
[6] A. Vertes, R.D. Levine, Chem. Phys. Lett. 171 (1990) 284.
[7] P. Williams, R.W. Nelson, in: K.G. Standing, W. Ens (Eds.), Methods and Mechanisms for Producing Ions from Large Molecules, Plenum Press, New York, 1991, p. 265.
[8] K. Dreisewerd, M. Schürenberg, M. Karas, F. Hillenkamp, Int. J. Mass Spectrom. Ion Processes 141 (1995) 127.
[9] R.C. Beavis, B.T. Chait, Chem. Phys. Lett. 181 (1991) 479.
[10] R. Braun, P. Hess, J. Chem. Phys. 99 (1993) 8330.
[11] A. Bencsura, A. Vertes, Chem. Phys. Lett. 247 (1995) 142.
[12] A. Bencsura, V. Navale, M. Sadeghi, A. Vertes, Rapid Commun. Mass Spectrom. 11 (1997) 679.
[13] X. Wu, M. Sadeghi, A. Vertes, J. Phys. Chem. B 102 (1998) 4770.
[14] Ł. Dutkiewicz, R.E. Johnson, A. Vertes, R. Pędrys, J. Phys. Chem. A 103 (1999) 2925.
[15] M. Sadeghi, X. Wu, A. Vertes, J. Phys. Chem. B 105 (2001) 2578.
[16] L.V. Zhigilei, P.B.S. Kodali, B.J. Garrison, J. Phys. Chem. B 101 (1997) 2028.
[17] L.V. Zhigilei, P.B.S. Kodali, B.J. Garrison, Chem. Phys. Lett. 276 (1997) 269.
[18] L.V. Zhigilei, B.J. Garrison, Appl. Phys. Lett. 71 (1997) 551.
[19] L.V. Zhigilei, P.B.S. Kodali, B.J. Garrison, J. Phys. Chem. B 102 (1998) 2845.
[20] L.V. Zhigilei, B.J. Garrison, Rapid Commun. Mass Spectrom. 12 (1998) 1273.

[21] P.B.S. Kodali, L.V. Zhigilei, B.J. Garrison, Nucl. Instrum. Methods Phys. Res. B 153 (1999) 167.
[22] L.V. Zhigilei, B.J. Garrison, Appl. Phys. Lett. 74 (1999) 1341.
[23] L.V. Zhigilei, B.J. Garrison, Mater. Res. Soc. Symp. Proc. 538 (1999) 491.
[24] L.V. Zhigilei, B.J. Garrison, Appl. Phys. A 69 (1999) S75.
[25] L.V. Zhigilei, B.J. Garrison, J. Appl. Phys. 88 (2000) 1281.
[26] Y.G. Yingling, L.V. Zhigilei, B.J. Garrison, A. Koubenakis, J. Labrakis, S. Georgiou, Appl. Phys. Lett. 78 (2001) 1631.
[27] A.G. Zhidkov, L.V. Zhigilei, A. Sasaki, T. Tajima, Appl. Phys. A 73 (2001) 741.
[28] http://galilei.chem.psu.edu//Research_abl.html; http://www.people.virginia.edu/~lz2n/Ablation.html.
[29] S. Woutersen, H.J. Bakker, Nature 402 (1999) 507.
[30] J.C. Deàk, L.K. Iwaki, S.T. Rhea, D.D. Dlott, J. Raman Spectr. 31 (2000) 263.
[31] H. Kim, D. Dlott, J. Chem. Phys. 94 (1991) 8203.
[32] H. Kim, Y. Won, J. Phys. Chem. 100 (1996) 9495.
[33] R.E. Wyatt, C. Iung, C. Leforestier, Acc. Chem. Res. 28 (1995) 423.
[34] B.J. Garrison, R. Srinivasan, J. Appl. Phys. 57 (1985) 2909.
[35] D. Fenyö, B.U.R. Sundqvist, B.R. Karlsson, R.E. Johnson, Phys. Rev. B 42 (1990) 1895.
[36] Y.G. Yingling, L.V. Zhigilei, B.J. Garrison, Nucl. Instrum. Methods Phys. Res. B 180 (2001) 171.
[37] Y.G. Yingling, L.V. Zhigilei, B.J. Garrison, J. Photochem. Photobiol. A Chem. 145 (2001) 467.
[38] V.A. Likhachev, A.I. Mikhailin, L.V. Zhigilei, Phil. Mag. A 69 (1994) 421.
[39] D.A. Allwood, R.W. Dreyfus, I.K. Perera, P.E. Dyer, Rapid Commun. Mass Spectrom. 10 (1996) 1575.
[40] K. Dreisewerd, M. Schürenberg, M. Karas, F. Hillenkamp, Int. J. Mass Spectrom. Ion Processes 154 (1996) 171.
[41] K. Riahi, G. Bolbach, A. Brunot, F. Breton, M. Spiro, J.-C. Blais, Rapid Commun. Mass Spectrom. 8 (1994) 242.
[42] I. Itzkan, D. Albagli, B.J. Banish, M. Dark, C. von Rosenberg, L.T. Perelman, G.S. Janes, M.S. Feld, AIP Conf. Proc. 288 (1994) 491.
[43] I. Itzkan, D. Albagli, M.L. Dark, L.T. Perelman, C. von Rosenberg, M.S. Feld, Proc. Natl. Acad. Sci. U.S.A. 92 (1995) 1960.
[44] V. Venugopalan, N.S. Nishioka, B.B. Mikić, Biophys. J. 69 (1995) 1259.
[45] A.A. Oraevsky, R. Esenaliev, S.L. Jacques, F.K. Tittel, SPIE Proc. Series 2391 (1995) 300.
[46] R. Cramer, R.F. Haglund Jr., F. Hillenkamp, Int. J. Mass Spectrom. Ion Processes. 169/170 (1997) 51.
[47] R.S. Dingus, R.J. Scammon, SPIE Proc. Series. 45 (1991) 1427.
[48] The initial temperature is zero in the simulations presented in this work. Results from the simulations with initial temperatures of 500 K do support the physical picture of the material ejection. These results are presented in Ref. [24].
[49] R. Srinivasan, B. Braren, Chem. Rev. 89 (1989) 1303.
[50] L.V. Zhigilei, Mater. Res. Soc. Symp. Proc. 677 (2001) AA2.1.1.
[51] L.V. Zhigilei, Appl. Phys. A, in press.
[52] M. Handschuh, S. Nettesheim, R. Zenobi, Appl. Surf. Sci. 137 (1999) 125.
[53] S.M. Hankin, P. John, J. Phys. Chem. B 103 (1999) 4566.
[54] I. Fournier, A. Brunot, J.C. Tabet, G. Bolbach, Int. J. Mass Spectrom. 213 (2001) 203.
[55] A.N. Krutchinsky, B.T. Chait, J. Am. Soc. Mass Spectrom. 13 (2002) 129.
[56] M. Karas, U. Bahr, F. Hillenkamp, Int. J. Mass Spectrom. Ion Processes 92 (1989) 231.
[57] V. Karbach, R. Knochenmuss, Rapid Commun. Mass Spectrom. 12 (1998) 968.
[58] M. Karas, M. Glückmann, J. Schäfer, J. Mass Spectrom. 35 (2000) 1.
[59] K.H. Song, X. Xu, Appl. Surf. Sci. 127–129 (1998) 111.
[60] M. Macler, M.E. Fajardo, Appl. Phys. Lett. 65 (1994) 2275.
[61] J. Heitz, J.T. Dickenson, Appl. Phys. A 68 (1999) 515.
[62] B.N. Kozlov, B.A. Mamyrin, Tech. Phys. 44 (1999) 1073.
[63] T.E. Itina, L.V. Zhigilei, B.J. Garrison, Nucl. Instrum. Methods Phys. Res. B 180 (2001) 238.
[64] T.E. Itina, L.V. Zhigilei, B.J. Garrison, J. Phys. Chem. B 106 (2002) 303.
[65] W. Ens, Y. Mao, F. Mayer, K.G. Standing, Rapid Commun. Mass Spectrom. 5 (1991) 117.
[66] T. Huth-Fehre, C.H. Becker, Rapid Commun. Mass Spectrom. 5 (1991) 378.
[67] P. Juhasz, M.L. Vestal, S.A. Martin, J. Am. Soc. Mass Spectrom. 8 (1997) 209.
[68] Y. Pan, R.J. Cotter, Org. Mass Spectrom. 27 (1992) 3.
[69] W. Zhang, B.T. Chait, Int. J. Mass. Spectrom. Ion Processes 160 (1997) 259.
[70] M. Glückmann, M. Karas, J. Mass Spectrom. 34 (1999) 467.
[71] D.R. Ermer, M. Baltz-Knorr, R.F. Haglund Jr, J. Mass Spectrom. 36 (2001) 538.
[72] S. Berkenkamp, C. Menzel, F. Hillenkamp, K. Dreisewerd, J. Am. Soc. Mass Spectrom. 13 (2002) 209.
[73] Y. Dou, L.V. Zhigilei, N. Winograd, B.J. Garrison, private communication.
[74] I.K. Perera, D. Allwood, P.E. Dyer, G.A. Oldershaw, Int. J. Mass Spectrom. Ion Processes 145 (1995) L9.
[75] I.K. Perera, D. Allwood, P.E. Dyer, G.A. Oldershaw, J. Mass Spectrom. 30 (1995) S3.
[76] G.R. Kinsel, R.D. Edmondson, D.H. Russell, J. Mass Spectrom. 32 (1997) 714.
[77] J.W. Elam, D.H. Levy, J. Phys. Chem. B 102 (1998) 8113.
[78] F. Aksouh, P. Chaurand, C. Deprun, S. Dellanegra, J. Hoyes, Y. Lebeyec, R.R. Pinho, Rapid Commun. Mass Spectrom. 9 (1995) 515.
[79] J.W. Elam, D.H. Levy, J. Chem. Phys. 106 (1997) 10368.
[80] P.H. Kobrin, G.A. Schick, J.P. Baxter, N. Winograd, Rev. Sci. Instrum. 57 (1986) 1354.
[81] Y. Tsuboi, K. Hatanaka, H. Fukumura, H. Masuhara, J. Phys. Chem. A 102 (1998) 1661.
[82] A.A. Oraevsky, S.L. Jacques, F.K. Tittel, J. Appl. Phys. 78 (1995) 1281.
[83] G. Paltauf, H. Schmidt-Kloiber, Appl. Phys. A 62 (1996) 303.

[84] D. Kim, C.P. Grigoropoulos, Appl. Surf. Sci. 127–129 (1998) 53.
[85] A. Karabutov, N. Podymova, V. Letokhov, SPIE Proc. Series 2624 (1996) 93.
[86] K. Dreisewerd, C. Menzel, A. Rolhfing, F. Hillenkamp, L.M. Kukreja, Proceedings of the 48th ASMS Conference on Mass Spectrometry and Allied Topics, Long Beach, CA, 11–15 June 2000.
[87] D. Feldhaus, C. Menzel, S. Berkenkamp, F. Hillenkamp, K. Dreisewerd, J. Mass Spectrom. 35 (2000) 1320.
[88] L.V. Zhigilei, B.J. Garrison, Appl. Surf. Sci. 127–129 (1998) 142.
[89] L.V. Zhigilei, B.J. Garrison, Proc. SPIE 3254 (1998) 135.
[90] T.A. Schoolcraft, G.S. Constable, L.V. Zhigilei, B.J. Garrison, Anal. Chem. 72 (2000) 5143.
[91] T.A. Schoolcraft, G.S. Constable, B. Jackson, L.V. Zhigilei, B.J. Garrison, Nucl. Instrum. Methods Phys. Res. B. 180 (2001) 245.
[92] S.L. Jacques, A.A. Oraevsky, R. Thompson, B.S. Gerstman, Proc. SPIE 2134A (1994) 54.
[93] C.P. Lin, M.W. Kelly, Proc. SPIE 2975 (1997) 174.
[94] C.P. Lin, M.W. Kelly, S.A.B. Sibayan, M.A. Latina, R.R. Anderson, IEEE J. Select. Topics Quantum Electron. 5 (1999) 963.
[95] C.R. Thompson, B.S. Gerstman, S.L. Jacques, M.E. Rogers, Bull. Math. Biol. 58 (1996) 513.
[96] X. Wen, D.E. Hare, D.D. Dlott, Appl. Phys. Lett. 64 (1994) 184.
[97] C.A. Noble, K.A. Prather, Environ. Sci. Technol. 30 (1996) 2667.
[98] D.T. Suess, K.A. Prather, Chem. Rev. 99 (1999) 3007.
[99] J.O. Allen, D.P. Fergenson, E.E. Gard, L.S. Hughes, B.D. Morrical, M.J. Kleeman, D.S. Gross, M.E. Gälli, K.A. Prather, G.R. Cass, Environ. Sci. Technol. 34 (2000) 211.
[100] D.B. Kane, M.V. Johnston, Anal. Chem. 73 (2001) 5365.
[101] M. Karas, D. Bachmann, F. Hillenkamp, Anal. Chem. 57 (1985) 2935.
[102] Cover Story, Time Magazine, 11 October, 1999.